3782 *J. Med. Chem.* **2010,** *53,* 3782–3792
DOI: 10.1021/jm100190c

Journal of
Medicinal
Chemistry
Article

Liposomal Formulation of Retinoids Designed for Enzyme Triggered Release

Palle J. Pedersen,[†] Sidsel K. Adolph,[|] Arun K. Subramanian,[†] Ahmad Arouri,[‡] Thomas L. Andresen,[§] Ole G. Mouritsen,[‡] Robert Madsen,[†] Mogens W. Madsen,[|] Günther H. Peters,[†] and Mads H. Clausen*,[†]

[†]*Department of Chemistry, Technical University of Denmark, Kemitorvet, Building 201 and 207, DK-2800 Kgs. Lyngby, Denmark,* [‡]*Department of Physics and Chemistry, MEMPHYS−Center for Biomembrane Physics, University of Southern Denmark, Campusvej 55, DK-5230 Odense M, Denmark,* [§]*Department of Micro- and Nanotechnology, Technical University of Denmark, DK-4000 Roskilde, Denmark, and* [|]*LiPlasome Pharma A/S, Technical University of Denmark, Diplomvej 378, DK-2800 Kgs. Lyngby, Denmark*

Received February 12, 2010

The design of retinoid phospholipid prodrugs is described based on molecular dynamics simulations and cytotoxicity studies of synthetic retinoid esters. The prodrugs are degradable by secretory phospholipase A_2 IIA and have potential in liposomal drug delivery targeting tumors. We have synthesized four different retinoid phospholipid prodrugs and shown that they form particles in the liposome size region with average diameters of 94−118 nm. Upon subjection to phospholipase A_2, the lipid prodrugs were hydrolyzed, releasing cytotoxic retinoids and lysolipids. The formulated lipid prodrugs displayed IC_{50} values in the range of 3−19 μM toward HT-29 and Colo205 colon cancer cells in the presence of phospholipase A_2, while no significant cell death was observed in the absence of the enzyme.

Introduction

Retinoids,[1] such as all-*trans* retinoic acid (ATRA,[a] Figure 1), are known for their broad and diverse biological functions, and various strategies have been explored to make retinoids applicable as drugs in the treatment of diseases.[2] One of the biological functions of ATRA is its anticancer activity toward a broad range of cancer types, like breast, prostate, and colon cancer.[3] For example, orally administrated ATRA is used clinically in the treatment of leukemia.[4] However, the oral administration route is restricted by a relative low bioavailability[4c] and a fast clearance from the bloodstream,[5] and thus alternative ways of administrating ATRA would be beneficial. Intravenous administration is hampered by the low water solubility of ATRA, but this can be circumvented by formulating ATRA in liposome based drug delivery systems.[6] Unfortunately, the liposomal formulation strategies have often been plagued by problems with leakage, which have led to an uncontrolled release of ATRA from the carrier system. Recently, we have introduced new liposomal drug delivery systems[7] that address the formulation challenges of relatively hydrophobic drugs. The drug delivery systems consist of secretory phospholipase A_2 ($sPLA_2$) IIA sensitive phospholipids and are constructed of drug−lipid prodrugs, in which the lipophilic anticancer drugs are covalently attached to the phospholipids. Despite successful incorporation of the well-known anticancer drug chlorambucil in the *sn*-2 position,[7a] it was later experienced that the desired delivery of free ATRA was not feasible due to lack of $sPLA_2$ activity on substrates like **1** (Figure 1).[7b] ATRA is a rigid molecule and contains a methyl substituent in close proximity to the carboxylic acid moiety. These features contrast with naturally occurring fatty acids, which are predominantly saturated and flexible molecules without branching. Knowing that some esters and amides of ATRA retain their activity,[8] we decided to incorporate an aliphatic C_6-linker between ATRA and the lipid backbone (Figure 2). To gain further insight into the substrate specificity of the $sPLA_2$ enzyme, hydrolysis of the lipid prodrugs was investigated by molecular dynamics (MD) simulation, which has earlier been demonstrated as a valuable tool for assessing $sPLA_2$ activity toward a range of substrates.[9]

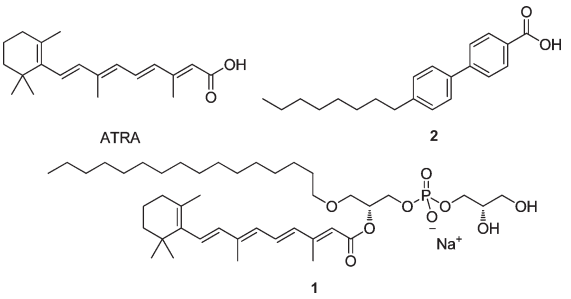

Figure 1. Structure of the cytotoxic compounds ATRA and **2** and the ATRA phospholipid prodrug (**1**) that is not hydrolyzed by $sPLA_2$.[7b]

One major drawback in applying ATRA as a drug is its nonselective activation of retinoic acid receptor (RAR) subtypes (RARs, α, β, γ), retinoic X receptor subtypes (RXRs, α,

*To whom correspondence should be addressed. Phone: +45 45252131. Fax: +45 45933968. E-mail: mhc@kemi.dtu.dk.

[a] Abbrevations: ATRA, all-*trans* retinoic acid; $sPLA_2$, secretory phospholipase A_2; MD, molecular dynamics; RAR, retinoic acid receptor; RXR, retinoic X receptor; rmsd, root-mean-square deviation; S, substrate; PMB, *p*-methoxybenzyl; DDQ, 2,3-dichloro-5,6-dicyano-1,4-benzoquinone; DBU, 1,8-diazabicyclo[5.4.0]undec-7-ene; DIAD, diisopropyl azodicarboxylate; NBS, *N*-bromosuccinimide; DLS, dynamic light scattering; DPPG, 1,2-dipalmitoyl-*sn*-glycero-3-phosphoglycerol; DSPG, 1,2-distearoyl-*sn*-glycero-3-phosphoglycerol; 1-*O*-DSPG, 1-*O*-stearyl-2-stearoyl-*sn*-glycero-3-phosphoglycerol; POPG, 1-palmitoyl-2-oleoyl-*sn*-glycero-3-phosphoglycerol; NBD-DPPE, 1,2-dipalmitoyl-*sn*-glycero-3-phosphoethanolamine-*N*-[7-nitro-2-1,3-benzoxadiazol-4-yl]; MALDI-TOF, matrix-assisted laser desorption/ionization time-of-flight; DHB, 2,5-dihydroxybenzoic acid; MTT, 3-(4,5-dimethylthiazolyl)-2,5-diphenyltetrazolium bromide.

 Published on Web 04/20/2010

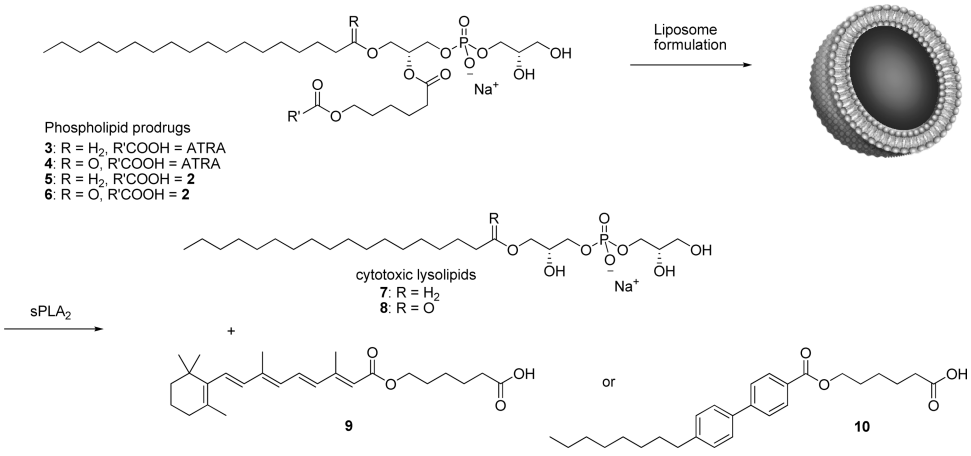

Figure 2. The $sPLA_2$ degradable phospholipid prodrugs **3**−**6**, with an aliphatic C_6-linker incorporated between the drug, R′COOH (ATRA or **2**), and the lipid backbone.

β, γ), and/or the subtype RAR isoforms, α1, α2, β1−β5, γ1, and γ2.[3a,10] The lack of selectivity is believed to be responsible for the severe side effects that have been observed during chronic administration of ATRA,[10] and therefore there is much interest in discovering more selective RAR agonists.[11] Targeting of RARβ2 has been found to have a suppressive effect on human tumors,[12] and recently 4-(4-octylphenyl)-benzoic acid (**2**, Figure 1) was identified as a selective RARβ2 agonist.[13] The lipophilicity of **2** makes it is a good candidate for incorporation into a liposomal drug delivery system through covalent attachment to the lipid backbone. However, since Bonsen et al. have demonstrated that benzoic acid is not released from the *sn*-2-position by $sPLA_2$,[14] direct attachment of **2** to the phospholipids was ruled out. Instead, we decided to investigate how attachment of an aliphatic C_6-linker would influence the cytotoxicity of **2** and the $sPLA_2$ activity toward the corresponding prodrug.

The retinoid−lipid prodrugs are designed to include the phosphatidylglycerol headgroup because human $sPLA_2$ IIA has strong affinity for negatively charged phospholipids.[15] The lipid backbone of the prodrugs contains either an *sn*-1-ester or an *sn*-1-ether functionality. Upon activation of $sPLA_2$, the prodrugs will be converted into the free drug and lysolipids (Figure 2) and while *sn*-1-ether lysolipids have good metabolic stability and are cytotoxic against many cell lines,[16] *sn*-1-ester lysolipids are rapidly metabolized (by e.g., lysophospholipases) and have been dismissed as suitable lysolipid drug candidates.[16a] Information about the cytotoxicity of *sn*-1-ester lysolipids is limited and covers only lysophosphatidylcholine lipids,[17] but these lipids have shown to be slightly better substrates for $sPLA_2$ than *sn*-1-ether lipids.[18] Therefore, we found it interesting to synthesize both types of prodrugs in order to study their relative hydrolysis rate and cytotoxicity.

Molecular Dynamics Simulations

Molecular dynamics (MD) simulations were performed to understand why **1** is not hydrolyzed by $sPLA_2$[7b] and which structural modification(s) of the prodrug would regain enzymatic hydrolysis. Simulations were carried out for $sPLA_2$−DPPG, $sPLA_2$−**1**, and as discussed below also for $sPLA_2$−**3** and $sPLA_2$−**5**. Simulations for each complex were repeated five times to estimate the statistical uncertainties in the calculated quantities. The stability of the simulations of the different $sPLA_2$ complexes were checked by computing the

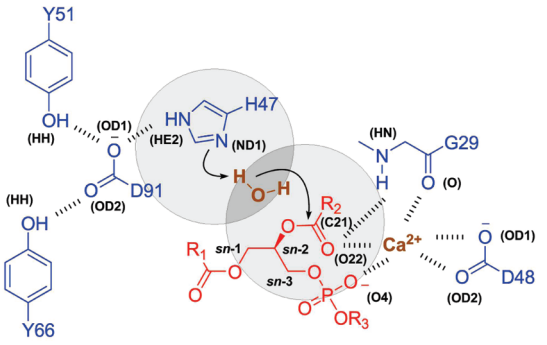

Figure 3. Representation of the active site in $sPLA_2$ with hydrogen bonds and ionic interactions indicated with dashed bonds. Key protein residues are drawn in blue, the substrate in red, and the calcium ion and the water molecule both in brown. The two gray circles indicate the *H*−*S* region, where the overlap in dark gray represents the water count region. Labels are shown in black, and atom types indicated in parentheses refer to the Protein Data Bank nomenclature.

time evolution of the root-mean-square deviation (rmsd) of the Cα atoms with respect to the protein structure obtained after minimization. Stable rmsd data were obtained after 1−2 ns for the $sPLA_2$−DPPG, $sPLA_2$−**3** and $sPLA_2$−**5** complexes reaching a plateau of ∼1.4 Å (Supporting Information). rmsd data for the $sPLA_2$−**1** complex were not stable, increasing to ∼2.5 Å after ∼6.5 ns (Supporting Information).

A prerequisite for successful hydrolysis is that a stable Michaelis−Menten complex is obtained and that a water molecule acting as a nucleophile can enter the catalytic cleft. To monitor the stability of the Michaelis−Menten complex, we have chosen distances according to their importance in the calcium-dependent enzymatic reaction.[19] The catalytic mechanism has been identified by X-ray crystallography, revealing that the catalytic device of $sPLA_2$ is essentially characterized by an aspartic acid−histidine dyad, a calcium-binding site, and a water molecule acting as the nucleophile. A schematic representation of the catalytic mechanism is shown in Figure 3, indicating that the calcium ion (cofactor) is coordinated to the D48 carboxylate groups (atoms: OD1 and OD2), the G29 carbonyl (O), the carbonyl (O22) in the substrate (S), and the phosphate (O4) in S. Atom types given in parentheses refer to the Protein Data Bank nomenclature. Furthermore, the catalytic residue, H47, is stabilized by D91,

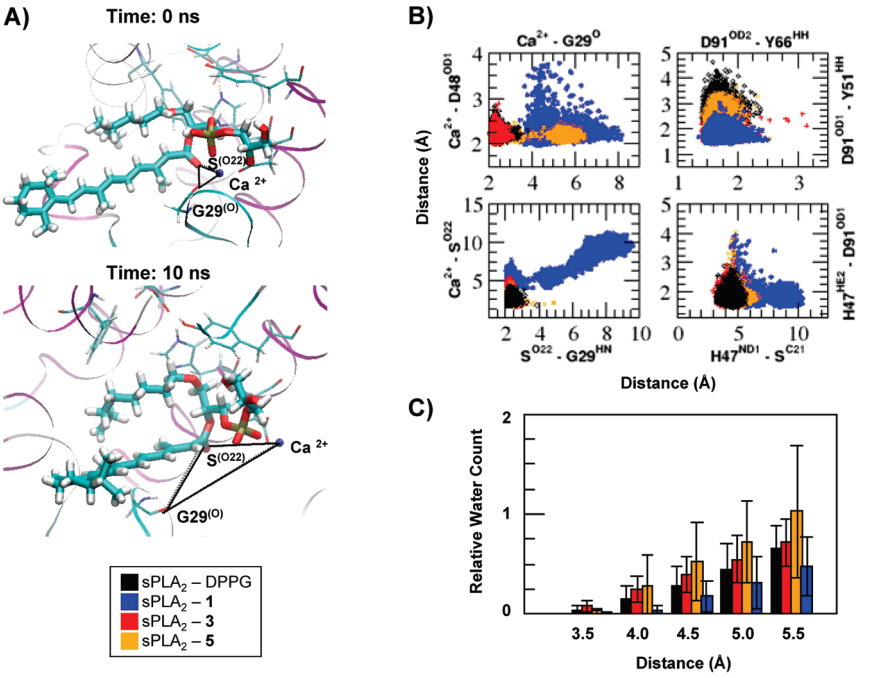

Figure 4. (A) ATRA induced structural perturbation of the Michaelis−Menten complex. Images taken at the beginning (top) and at the end (bottom) of an sPLA$_2$−**1** simulation revealed that ATRA induced conformational changes (as evident from the G29$^{(O)}$−Ca^{2+}−S$^{(O22)}$ distances indicated by the triangles) leading to the distortion of the Michaelis−Menten complex. (B) 2D scatter plots of distances between selected residue pairs important for stabilizing the Michaelis−Menten complex. (C) Histograms of relative water counts as a function of distance from both H47^{ND1} and S^{C21} (*H*−*S* region; Figure 3).

which forms hydrogen bonds with Y51 and Y66. The water molecule acting as the nucleophile enters the region between H47^{ND1} and S^{C21}. This region will be referred to as the *H*−*S* region (Figure 3).

We have checked the stability of the Michaelis−Menten complexes by monitoring the following distances during the simulations: Ca^{2+}−G29^{O}, Ca^{2+}−D48^{OD1}, Ca^{2+}−S^{O22}, S^{O22}−G29^{HN}, H47^{HE2}−D91^{OD1}, H47^{ND1}−S^{C21}, D91^{OD2}−Y66^{HH}, and D91^{OD1}−Y51^{HH}. The time evolution of these distances is provided in the Supporting Information, and 2D scatter plots are shown in Figure 4.

For prodrug **1**, no stable Michaelis−Menten complex could be observed, and hence in accordance with experimental data, no hydrolysis can occur. The rigid nature of the ATRA ester at the *sn*-2-position of the prodrug causes distortion of several distances involved in the Michaelis−Menten complex (Figure 4). For instance, distances Ca^{2+}−S^{O22} and G29^{HN}−S^{O22} are significantly larger for sPLA$_2$−**1** than sPLA$_2$−DPPG (Figure 4). The distortion is also highlighted by the images taken at the beginning and upon completion of an sPLA$_2$−**1** simulation, respectively (Figure 4). Introduction of a C$_6$-linker between the phospholipid backbone and **1** was sufficient to confer stability of the Michaelis−Menten complex in sPLA$_2$−**3** and sPLA$_2$−**5**.

Although a stable Michaelis−Menten complex could be obtained by introducing a C$_6$-linker, the question remained if water can reach the *H*−*S* region (Figure 3) in sPLA$_2$ complexed with **3** or **5**. To quantify the probability that water molecules enter the *H*−*S* region, we counted the number of water molecules within certain distances (d = 3 Å − 6 Å; Δd = 0.5 Å) from both H47^{ND1} and S^{C21}, and the counts were normalized by dividing the respective water counts by the water count determined at 6 Å (Figure 4). Averages and standard deviations of normalized water counts were calculated from the five simulations of each complex. The relative water counts extracted from sPLA$_2$−**3** and −**5** simulations were similar to those extracted from sPLA$_2$−DPPG simulations (Figure 4). Contrarily, the relative water counts extracted from sPLA$_2$−**1** were very low when compared to the other complexes. Because complexes of DPPG, **3**, and **5** show similar relative water counts and their Michaelis−Menten complexes are stable, these results predict that **3** and **5** will be hydrolyzed by sPLA$_2$.

Synthesis of Retinoid Esters

The linker moiety *tert*-butyl 6-hydroxyhexanoate (**11**)[20] was coupled with ATRA by a Mitsunobu reaction (Scheme 1),[21] which we previously have demonstrated as a reliable method for forming esters of ATRA.[7b] The following *tert*-butyl deprotection led to degradation of the ATRA skeleton under acidic conditions (5% TFA or $ZnBr_2$[22] in CH_2Cl_2 or HF in MeCN), but using 2,6-lutidine and TMSOTf in CH_2Cl_2[23] afforded the carboxylic acid **9** in a good yield (Scheme 1). The ATRA ester **9** was isolated as yellow crystals and was stable when stored at −20 °C under an inert atmosphere, whereas the oily *tert*-butyl ester of **9** decomposes upon less than one month of storage. This highlights the importance of storing ATRA-analogues as solids in order to avoid decomposition. The corresponding linker-molecule of **2**[24] was synthesized by a Steglich coupling[25] with **11** followed by a deprotection of the *tert*-butyl ester with TFA in CH_2Cl_2 (Scheme 1). In contrast to the ATRA-analogues, we never observed any decomposition of the synthetic derivatives of **2** neither as oils nor solids. The cytotoxicity of ATRA, **2**, **9**, and **10** were evaluated in three cell lines, and the retinoid esters had activities comparable to the acids (vide infra).

Synthesis of Lipid Prodrugs

The cytotoxicity of the esters **9** and **10** and the results from the MD simulations prompted us to proceed with the synthesis

Scheme 1. Synthesis of the Retinoid Esters[a]

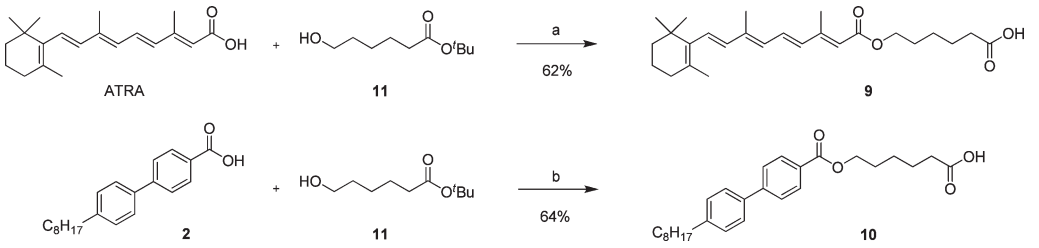

[a] Reagents: (a) (i) diisopropyl azodicarboxylate (DIAD), PPh_3, THF; (ii) TMSOTf, 2,6-lutidine, CH_2Cl_2; (b) (i) dicyclohexylcarbodiimide (DCC), DMAP, CH_2Cl_2; (ii) TFA, triisopropylsilane, CH_2Cl_2.

Scheme 2. Synthesis of the Lipid Precursors **15** and **18**[a]

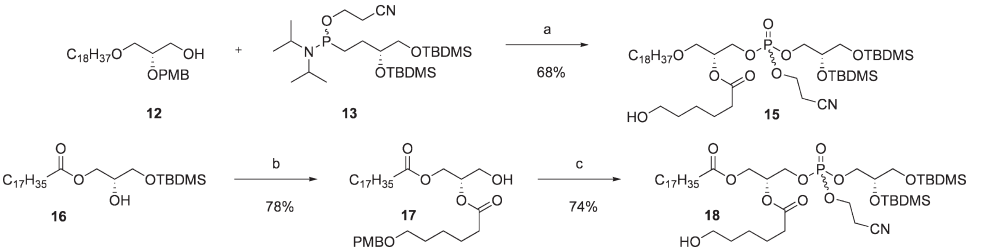

[a] Reagents: (a) (i) tetrazole, CH_2Cl_2, MeCN; (ii) ^{t}BuOOH; (iii) DDQ, H_2O, CH_2Cl_2; (iv) **14**, DCC, DMAP, CH_2Cl_2; (v) DDQ, H_2O, CH_2Cl_2; (b) (i) **14**, EDCI, DMAP, CH_2Cl_2; (ii) NBS, DMSO, THF, H_2O; (c) (i) **13**, tetrazole, CH_2Cl_2, MeCN; (ii) ^{t}BuOOH; (iii) DDQ, H_2O, CH_2Cl_2.

Scheme 3. Synthesis of the *sn*-1-Ether and *sn*-1-Ester prodrugs **3**, **4**, **5**, and **6**[a]

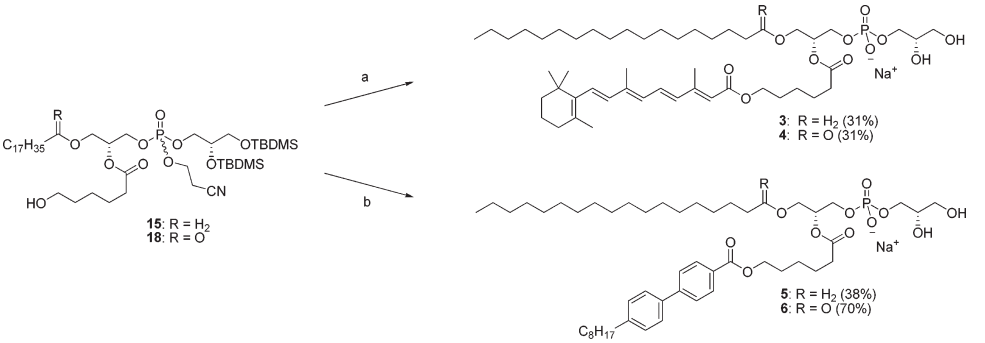

[a] Reagents: (a) (i) **15**, ATRA, DIAD, PPh_3, THF or **18**, ATRA, DCC, DMAP, Et_3N, Et_2O; (ii) DBU, CH_2Cl_2; (iii) HF, H_2O, CH_2Cl_2, MeCN; (b) (i) **2**, DCC, DMAP, CH_2Cl_2; (ii) DBU, CH_2Cl_2; (iii) HF, H_2O, CH_2Cl_2, MeCN.

of the corresponding *sn*-1-ether and *sn*-1-ester lipid prodrugs **3**−**6**. The backbone of the *sn*-1-ether prodrugs was constructed by a tetrazole mediated coupling of alcohol **12** and phosphoramidite **13**, followed by an oxidation of the phosphite to the phosphate with ^{t}BuOOH (Scheme 2).[7a] Deprotection of the *p*-methoxybenzyl (PMB) group in moist CH_2Cl_2 with 2,3-dichloro-5,6-dicyano-1,4-benzoquinone (DDQ) afforded the secondary alcohol, which was reacted with 6-(4-methoxybenzyloxy)-1-hexanoic acid (**14**) to give an ester. The newly introduced PMB-group was then removed, affording alcohol **15** in an overall yield of 51% (Scheme 2). Secondary alcohol **16**, synthesized from 2,3-*O*-isopropylidene-*sn*-glycerol according to the procedures by Gaffney et al[26] and Burgos et al.,[27] served as the starting material for the *sn*-1-ester prodrugs (Scheme 2). Diester **17** was obtained by coupling of **14** and **16**, and the following TBDMS deprotection was best achieved using *N*-bromosuccinimide (NBS) in a mixture of DMSO, THF, and H_2O (Scheme 2),[27,28] while alternative conditions like Bu_4NF and imidazole in THF[29] or HF in MeCN led to a significant degree of acyl migration. Mosher ester analysis[30] of **17** showed that the enantiomeric purity was >95%. The phosphate headgroup was attached in the same way as for the *sn*-1-ether lipids, and PMB deprotection gave the primary alcohol **18** (Scheme 2). Phospholipids **15** and **18** were converted to the desired prodrugs of ATRA and **2** (Scheme 3). The ATRA moiety was introduced either by the Mitsunobu reaction or the Steglich coupling, and the final prodrugs **3** and **4** were obtained after removal of the cyanoethyl group with 1,8-diazabicyclo[5.4.0]undec-7-ene (DBU) and TBDMS-deprotection mediated by HF in MeCN/CH_2Cl_2/H_2O. Prodrugs **5** and **6** were accessed by coupling between **2** and the primary alcohols **15** and **18**, after which the remaining chemistry was similar to the synthesis of **3** and **4** (Scheme 3). ^{31}P NMR of the synthesized prodrugs showed one signal resonating between −1 ppm and 2 ppm, demonstrating high diastereomeric and regioisomeric purity (>95%).

Biophysical Characterization

The lipid prodrugs (**3**−**6**) were formulated as liposomes by extrusion in HEPES buffer using the dry lipid film technique,[31] yielding clear solutions. The particle size of the formulated

Table 1. Measurement of Particle Size with DLS

	particle size	
prodrug	diameter (nm)	polydispersity index
3	94	0.08
4	97	0.13
5	118	0.16
6	118	0.05

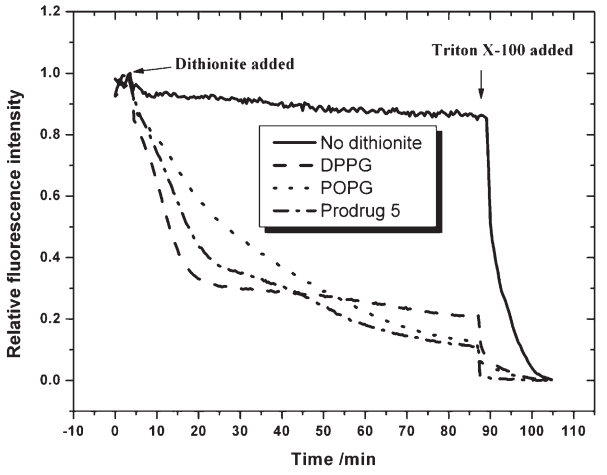

Figure 5. Time-dependent fluorescence from NBD labeled lipids quenched by dithionite.

lipids was measured by dynamic light scattering (DLS). The DLS analysis revealed that all of the lipids were able to form particles with a diameter around 100 nm (Table 1 and Supporting Information) and with a low polydispersity, indicating the formation of unilamellar vesicles. The formation of a unilamellar bilayer is further supported by the fluorometric procedure described by McIntyre et al.,[32] which was used to study the permeability. Vesicles formed from prodrug **5** was compared to vesicles of 1,2-dipalmitoyl-*sn*-glycero-3-phosphoglycerol (DPPG) and 1-palmitoyl-2-oleoyl-*sn*-glycero-3-phosphoglycerol (POPG). The lipids were formulated with 1,2-dipalmitoyl-*sn*-glycero-3-phosphoethanolamine-*N*-[7-nitro-2-1,3-benzoxadiazol-4-yl] (NBD-DPPE, 0.15 mol %). The fluorescence of the NBD group was monitored over time before and after the addition of dithionite ($S_2O_4^{-2}$), which functions as a quenching agent. At the end of the experiment, the detergent Triton X-100 was added to solubilize the lipid vesicles and cause 100% quenching (see Figure 5). As evident from the figure, the decrease in the fluorescence of the NBD-labeled gel-state DPPG occurs in two distinct steps, an immediate and fast one completed after 20 min followed by much slower decay of fluorescence. We anticipate that the quick drop in fluorescence signal corresponds to quenching of the dye in the outer leaflet and is dependent on the fraction of lipids exposed to the surrounding, i.e., vesicle size and lamellarity. The slower second step is due to quenching of the dye in the inner leaflet, which is controlled by membrane permeability to dithionite. In the case of the fluid POPG vesicles, the quenching of both leaflets occurs simultaneously, resulting effectively in a single exponential-like decay in the NBD fluorescence. A comparable behavior for gel-state and fluid membranes has been reported previously.[32,33] The quenching of the NBD-labeled vesicles for prodrug **5** resembles that of DPPG, demonstrating that **5** forms a bilayer membrane, however seemingly more permeable to dithionite than the vesicles of DPPG.

Differential scanning calorimetry scans (15−65 °C) of the lipid solutions of **3** and **5** displayed no gel-to-liquid crystalline or any other thermotropic phase transition in the tested temperature range (data not shown), indicating that the lipid bilayers are in a fluid state. This was not surprising taking into account the bulky and stiff nature of the substituents in the *sn*-2-position, which hampers well-ordered chain packing.

The ability of $sPLA_2$ to hydrolyze the formulated lipids at 37 °C was investigated with matrix-assisted laser desorption/ionization time-of-flight (MALDI-TOF) MS. MALDI-TOF MS is a fast and sensitive technique which has been shown to be a reliable tool for detection of lipids.[34] In Figure 6, the obtained MS data for the *sn*-1-ether prodrug **3** subjected to purified $sPLA_2$ from snake (*Agkistrodon piscivorus piscivorus*) venom is shown. Gratifyingly, and as evident from the spectra (Figure 6), the prodrug ($M + H^+$) is consumed by the enzyme and the desired constituents, lysolipid **7** ($M + H^+$) and ATRA ester **9** ($M + Na^+$), are released. The MALDI-TOF MS analysis of the *sn*-1-ether prodrugs **3** and **5** and the *sn*-1-ester prodrugs **4** and **6** revealed that all of the prodrugs were degraded by the enzyme (Table 2) and the desired molecules were released (see Supporting Information). The observation that the *sn*-1-ether prodrugs were consumed by $sPLA_2$ to the same extent as the *sn*-1-ester prodrugs illustrate and confirm that *sn*-1-ether phospholipids are excellent substrates for $sPLA_2$. On the basis of the MALDI-TOF MS analysis of the $sPLA_2$ activity on the various prodrugs, we can conclude that the incorporation of an aliphatic C_6-linker between ATRA and the lipid backbone resolved the issue of $sPLA_2$ activity on ATRA-lipid prodrugs. The experimental observations are in agreement with the outcome from the MD simulations, illustrating the power and potential of using MD simulations in the design of $sPLA_2$ degradable lipid prodrugs. To rule out that the degradation of the prodrugs was caused by nonenzymatic hydrolysis, a sample of each prodrug was subjected to the reaction conditions in the absence of $sPLA_2$. As evident from the spectra in Figure 6 (and in Supporting Information), no degradation of the prodrugs was observed within 48 h and none of the release products were detectable. Finally, we compared the enzyme activity of the purified $sPLA_2$ from snake (*Agkistrodon piscivorus piscivorus*) venom with the commercially available $sPLA_2$ from snake (*Naja mossambica mossambica*) venom, and as can be seen in Table 2, the two enzymes perform equally well on all substrates.

Fawzy et al.[35] and Hope et al.[36] have demonstrated two decades ago that ATRA is an inhibitor for $sPLA_2$, reporting IC_{50} values of < 50 and 10 μM respectively. However, we have later shown that DPPG is fully hydrolyzed by $sPLA_2$ in the presence of 0.1 and 1.0 equiv of ATRA,[7b] proving that the lack of hydrolysis for the ATRA-lipid prodrug **1** is not a consequence of inhibition by ATRA. These observations are further supported by the present work, in which it was found that **9** ($IC_{50} = 8\ \mu M$, $K_i = 6\ \mu M$, see Supporting Information) inhibits $sPLA_2$ at the same level as ATRA ($IC_{50} = 15\ \mu M$, $K_i = 11\ \mu M$), and whereas the ATRA-lipid prodrug **1** is not consumed by the enzyme, the prodrugs **3** and **4** are fully degraded. This demonstrates that under the conditions used, the released ATRA ester **9** does not inhibit $sPLA_2$, and the difference in degradation of the prodrugs therefore solely relies on the ability of $sPLA_2$ to hydrolyze the different prodrugs. Additionally, Cunningham et al. have reported K_i values < 100 nM[37] for potent $sPLA_2$ inhibitors, illustrating that ATRA and **9** are weak inhibitors.

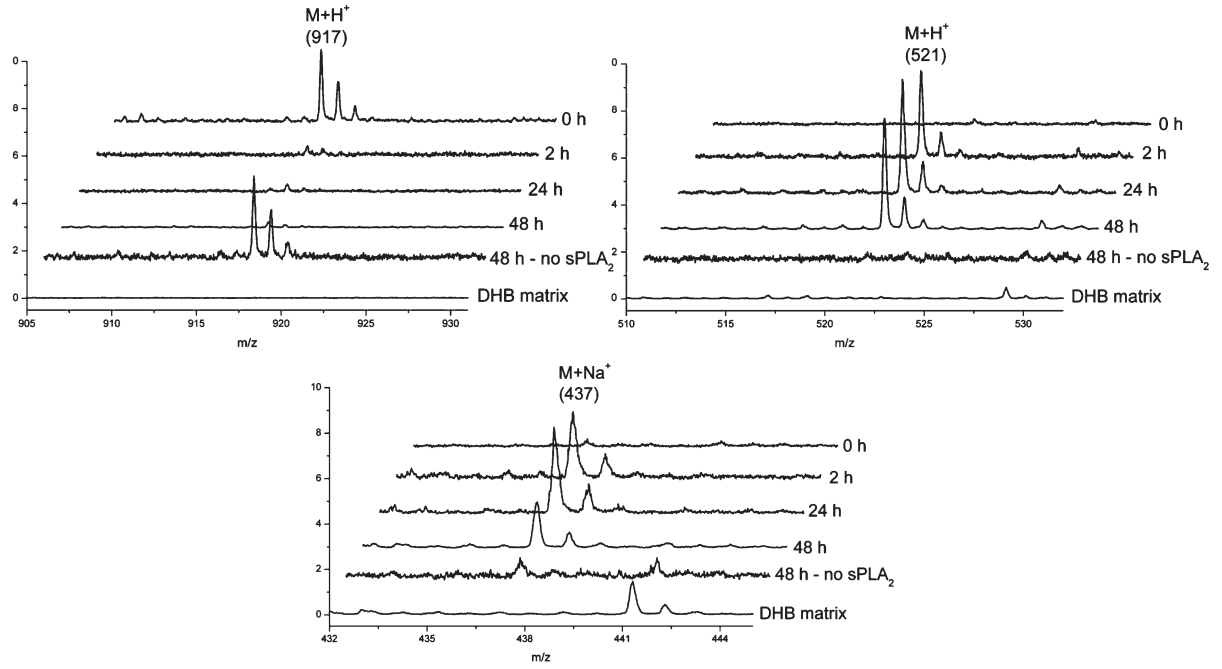

Figure 6. MALDI-TOF MS monitoring of snake (*Agkistrodon piscivorus piscivorus*) venom $sPLA_2$ activity on the *sn*-1-ether prodrug **3**. The spectra demonstrate that the prodrug **3** (top left) is consumed and that the lysolipid **7** (top right) and the ATRA ester **9** (bottom) are released.

Table 2. Measurement of $sPLA_2$ Activity on the Prodrugs by MALDI-TOF MS

	hydrolysis by $sPLA_2$[a]	
prodrug	*Agkistrodon piscivorus piscivorus*	*Naja mossambica mossambica*
3	+	nd
4	+	+
5	+[b]	+[b]
6	+	+

[a] Determined by MALDI-TOF MS after 48 h incubation at 37 °C with purified $sPLA_2$ from snake (*Agkistrodon piscivorus piscivorus* or *Naja mossambica mossambica*) venom. [b] After 48 h, a small signal for prodrug **5** remains; nd = not determined.

Cytotoxicity

The cytotoxicity of ATRA, **2**, **9**, and **10** were evaluated in MT-3 breast carcinoma, HT-29 colon carcinoma, and Colo205 colon adenocarcinoma cell lines (Table 3). Interestingly, the retinoid esters were either more active than ATRA and **2** or equal in potency in the tested cell lines. A possible explanation for the enhanced activity of these molecules is that the derivatization increases the lipophilicity of the drugs, augmenting transport over the cell membrane. RARβ2 agonists **2** and **10** showed very little activity against HT-29 cells, and presumably this is because growth inhibition in this cell line is induced by RARα agonists[38] and **2** has a low affinity for that receptor.[13] The result is also a strong indication that the cytotoxicity of **10** in MT-3 and Colo205 originate from RARβ2 activation.

The cytotoxicity of the prodrugs **3**−**6** was investigated in HT-29 colon carcinoma and Colo205 colon adenocarcinoma cells. HT-29 colon carcinoma cells do not secrete $sPLA_2$, which allowed us to test the activity in the presence and absence of $sPLA_2$. As evident from Table 4 and the dose−response curve for **3** and **5** (Figure 7), none of the prodrugs were able to induce significant cell death in the absence of $sPLA_2$, whereas upon $sPLA_2$ addition, all of the prodrugs displayed IC_{50} values below 10 μM in HT-29 cells and complete cell death was obtained when higher concentrations were applied (see Figure 7). Evidently, the cytotoxicity is induced by $sPLA_2$ triggered breakdown of the prodrugs into **9** or **10** and the lysolipids. Interestingly, we observed that the *sn*-1-ester prodrug **6** in the presence of $sPLA_2$ displayed almost the same cytotoxicity toward HT-29 cells as the corresponding *sn*-1-ether prodrug **5**, and taking the low activity of **10** in HT-29 cells

Table 3. IC_{50} (μM) Values for the Retinoids in Three Cancer Cell Lines[a]

compd	MT-3 IC_{50} (μM)	HT-29 IC_{50} (μM)	Colo205 IC_{50} (μM)
ATRA	30 ± 4	4.3 ± 0.2	37 ± 1
9	17 ± 1	3.6 ± 1.8	17 ± 2
2	51 ± 3	> 200	> 200
10	14 ± 1	> 200	127 ± 18

[a] Cytotoxicity was measured using the MTT assay as cell viability 48 h after incubation with the indicated substances for 24 h and shown by mean ± SD (n = 3).

Table 4. IC_{50} (μM) Values for the Prodrugs **3**−**6**, the Lysolipids **7** and **8**, DSPG, and 1-*O*-DSPG in HT-29 and Colo205 Cancer Cell Lines[a]

compd	HT-29 IC_{50} (μM)	HT-29 + $sPLA_2$[b] IC_{50} (μM)	Colo205 IC_{50} (μM)
3	> 200	7 ± 2	16 ± 4
4	> 200	6 ± 1	12 ± 3
5	> 200	3 ± 1	7 ± 6
6	> 200	8 ± 1	19 ± 4
7	11 ± 6	nd	25 ± 2
8	7 ± 1	nd	22 ± 3
DSPG	> 200	25 ± 11	54 ± 7
1-*O*-DSPG	> 200	9 ± 2	33 ± 4
$C_{17}H_{35}COOH$	> 200	nd	> 200
$sPLA_2$	*c*	*c*	*c*

[a] Cytotoxicity was measured using the MTT assay as cell viability 48 h after incubation with the indicated substances for 24 h and shown by mean ± SD ($n \geq 3$); nd = not determined. [b] Snake (*Agkistrodon piscivorus piscivorus*) venom $sPLA_2$ was added to a final concentration of 5 nM. [c] No change in cell viability was observed after 24 h.

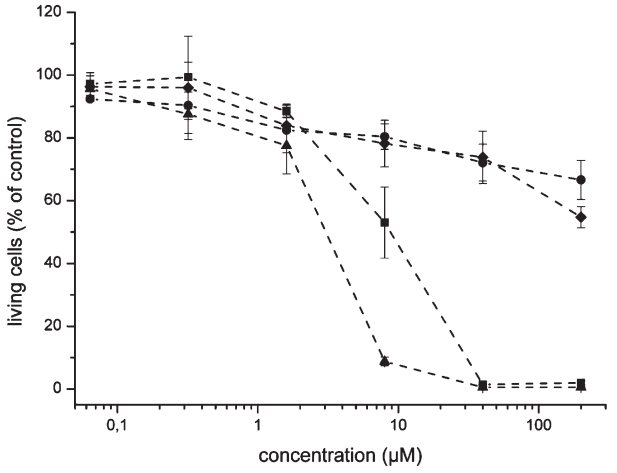

Figure 7. Dose−response curves for the treatment of HT-29 cells with the *sn*-1-ether prodrugs **3** (●), **3** + $sPLA_2$ (■), **5** (◆), and **5** + $sPLA_2$ (▲).

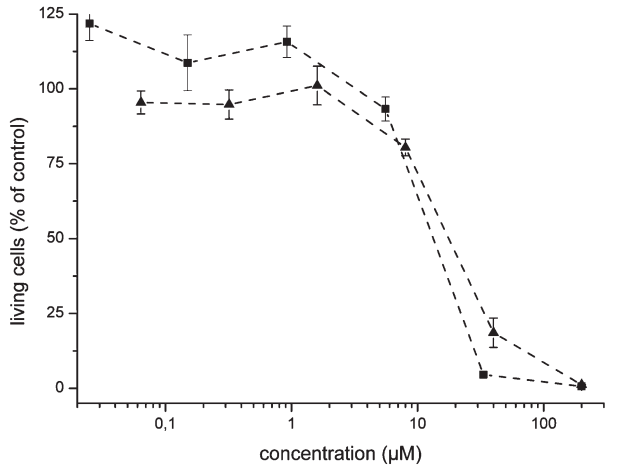

Figure 8. Dose−response curves for the treatment of Colo205 cells with *sn*-1-ester prodrugs **4** (■) and **6** (▲).

(Table 3) into account, these results indicate that *sn*-1-ester lysolipids (**8**) contribute with the same degree of potency as *sn*-1-ether lysolipids (**7**). These findings were verified when the free lysolipids **7** (see Supporting Information) and **8** were tested against HT-29 cells. Both lysolipids displayed IC_{50} values close to 10 μM, and similar results were obtained for DSPG and 1-*O*-stearyl-2-stearoyl-*sn*-glycero-3-phosphoglycerol (1-*O*-DSPG, see Supporting Information) in the presence of $sPLA_2$ (Table 4). We conclude that even though *sn*-1-ester lysolipids generally are rapidly metabolized, under these in vitro conditions, there is no significant metabolism of the lipid backbone and therefore we observe an equal potency of the two lysolipids. With the control experiments in hand, it is possible to determine the origin of the cytotoxicity of the prodrugs in HT-29 cells, and as evident from Tables 3 and 4, the majority of the activity arises from the lysolipids in prodrug **5** and **6** while for the prodrugs **3** and **4** there appear to be an equal contribution from the lysolipids (**7** and **8**) and the ATRA ester **9**. Colo205 cells express $sPLA_2$, and encouragingly, the four prodrugs induce cell death with IC_{50} values below 20 μM (Table 4) and complete cell death was obtained when higher concentrations were applied (see Figure 8), indicating that the secreted $sPLA_2$ in Colo205 cells provides the desired hydrolysis and release of the anticancer agents. Additionally, the prodrugs **3** and **4** displayed IC_{50} values below the free lysolipids but similar to **9**, indicating that the majority of the cytotoxicity can be ascribed to the released ATRA ester **9**. For prodrugs **5** and **6**, the IC_{50} values indicate a cumulative effect because these prodrugs are more potent than both of the released cytotoxic compounds by themselves, demonstrating the advantage of the prodrug formulation.

Conclusion

In the present study we have successfully synthesized lipid prodrugs of retinoids and demonstrated that they can be formulated as liposomes that are degraded by $sPLA_2$. On the basis of MD simulations, we incorporated a C_6-linker between the glycerol backbone of the lipids and the retinoids to overcome the lack of enzymatic activity stemming from the rigid nature of ATRA and **2**. The resulting prodrugs **3**−**6** were hydrolyzed completely by $sPLA_2$ within 24 h and were demonstrated to be cytotoxic to cancer cells in the presence of the enzyme.

The liposomal formulation is very well suited for active substances with low water solubility, and the novel prodrugs present a solution to formulation of retinoids for applications in cancer therapy. Furthermore, our findings underpin the overall strategy of covalently linking cytotoxic compounds to lipids and widen the scope of the approach because even very sterically hindered substrates can now be effectively incorporated into liposomes and released through an enzyme-triggered degradation.

Experimental Section

General. Starting materials, reagents, and solvents were purchased from Sigma-Aldrich and used without further purification. POPG, DPPG, DSPG, 1-stearoyl-2-hydroxy-*sn*-glycero-3-phospho-(1′-*rac*-glycerol) (**8**), and NBD-DPPE were purchased from Avanti Polar Lipids (Alabaster, AL). The purified snake venom $sPLA_2$ from *Agkistrodon piscivorus piscivorus* was donated by Dr. R. L. Biltonen (University of Virginia), and $sPLA_2$ from *Naja mossambica mossambica* was purchased from Sigma-Aldrich. CH_2Cl_2 was dried over 4 Å molecular sieves, and THF was dried over sodium/benzophenone and distilled before use. Evaporation of solvents was done under reduced pressure (in vacuo). TLC was performed on Merck aluminum sheets precoated with silica gel 60 F_{254}. Compounds were visualized by charring after dipping in a solution of Ce(IV) (6.25 g of $(NH_4)_6Mo_7O_{24}$ and 1.5 g of $Ce(SO_4)_2$ in 250 mL of 10% aq H_2SO_4) or an ethanolic solution of phosphomolybdenic acid (48 g/L). Flash column chromatography was performed using Matrex 60 Å silica gel. The purity of all tested compounds was found to be >95% by HPLC (see Supporting Information). HPLC was performed on a Waters Alliance HPLC equipped with a DAD, using a LiChrospher Si 60 column and eluting with water/isopropanol/hexane mixtures.[39] NMR spectra were recorded using a Bruker AC 200 MHz spectrometer, a Varian Mercury 300 MHz spectrometer, or a Varian Unity Inova 500 MHz spectrometer. Chemical shifts were measured in ppm and coupling constants in Hz, and the field is indicated in each case. IR analysis was carried out on a Bruker Alpha FT-IR spectrometer, and optical rotations were measured with a Perkin-Elmer 341 polarimeter. HRMS was recorded on an Ionspec Ultima Fourier transform mass spectrometer.

Molecular Dynamics Simulations. The crystal structures of bee venom (*Apis Mellifera*) phospholipase A_2 complexed with the transition-state analogue, L-1-*O*-octyl-2-heptylphosphonyl-*sn*-glycero-3-phosphoethanolamine (diC8(2Ph)PE),[19] resolved to 2.0 Å, and human phospholipase A_2 IIA complexed with 6-phenyl-4(*R*)-(7-phenyl-heptanoylamino)-hexanoic acid,[40] resolved to 2.1 Å, were obtained from the Protein Data Bank[41] (entry codes: 1poc and 1kqu, respectively). The initial modeling step

involved placing diC8(2Ph)PE into the binding cleft of human phospholipase A_2 IIA, as described previously.[18] A previously assembled $sPLA_2$−substrate complex[18] was used as the template to place lipid prodrugs into the active site. The optimized lipid prodrugs were manually overlapped with the pre-existing substrate, which was subsequently deleted. NAMD software[42] with the Charmm27 all-atom parameter set and TIP3 water model was used for all simulations.[43] The lipid prodrugs were first energy-minimized for 1000 steps before using them in simulations. Missing force field parameters for the prodrug molecules were taken from similar atom types in the CHARMM27 force field. The $sPLA_2$−lipid complexes were solvated using the program SOLVATE.[44] Eighteen water molecules were randomly replaced with chloride ions to neutralize the systems. Ultimately, the system contained ∼4900 water molecules in a simulation cell of dimensions $52.7 \times 51.7 \times 67.3$ Å^3. An initial energy minimization of the complex was carried out for 1000 steps, and the system was further minimized for 100, 200, 300, 400, and 500 steps to generate different starting structures. Periodic boundary conditions were applied in x, y, and z directions. Initial MD simulations were conducted for ∼100 ps in which each system was slowly heated to 300 K. Simulations were carried out for 10 ns in the NPT ensemble, i.e., at constant number of atoms (N), pressure (P), and temperature (T). A time step of 1 fs and an isotropic pressure of 1 atm using the Langevin piston method[45] were employed. Electrostatic forces were calculated using the particle mesh Ewald method with a uniform grid spacing of ∼1 Å.[46] A 12 Å cutoff was used for terminating the van der Waals interactions in combination with a switching function starting at 10 Å. Analysis of the trajectories were performed using the Visualization Molecular Dynamics software suite.[47]

Liposome Preparation and Particle Size Determination. The lipid prodrugs **3**−**6** were dissolved in $CHCl_3$ in a glass tube and dried under vacuum for 15 h to form a thin film. The lipid prodrugs (2 mM) were solubilized by addition of aqueous buffer (0.15 M KCl, 30 μM $CaCl_2$, 10 μM EDTA, 10 mM HEPES, pH 7.5) and vortexed periodically over 1 h at 20 °C. Subsequently, the solutions were extruded through a 100 nm polycarbonate cutoff membrane (20−30 repetitions) using a Hamilton syringe extruder (Avanti Polar Lipids, Birmingham, AL). The particle size distribution of the formulated lipids was measured by DLS. The DLS measurements were obtained using a Zetasizer nano particle analyzer (ZS ZEN3600, Malvern Instrument, Westborough, MA).

Permeability Assay. The permeability of the lipid vesicles was examined using the procedure described by McIntyre et al.[32] The lipid vesicles were labeled with NBD-DPPE (0.15 mol %) and prepared in an aqueous buffer (10 mM HEPES, 1 M sucrose, 150 mM NaCl, pH 7.4) by sonication for 30 min at 45 °C and then extrusion through a 100 nm filter at 45 °C. Sucrose was added to minimize the osmolarity difference between the external solution and the vesicle interior that will arise after the addition of dithionite.[48] The experiments were performed in duplicates or more using FLUOstar Omega microplate reader (BMG LABTECH) in a 96-well microplate at 20 °C (150 μL). The lipid samples (100 μM) were allowed to equilibrate at 20 °C before the addition of sodium dithionite ($Na_2S_2O_4$) solution (33 mM), which was used as a quenching agent. Because of the high instability of dithionite,[49] the dithionite solution was freshly prepared prior to use. The NBD fluorescence was observed at 520 nm (ex 485 nm). After 85 min, Triton X-100 was added to the medium (0.3 wt %).

$sPLA_2$ Activity Measurements Monitored by MALDI-TOF MS. The formulated lipid prodrugs (0.40 mL, 2 mM) were diluted in an aqueous buffer (2.1 mL, 0.15 M KCl, 30 μM $CaCl_2$, 10 μM EDTA, 10 mM HEPES, pH 7.5), and the mixture was stirred at 37 °C in a container protected from light. The catalytic reaction was initiated by addition of snake (*Agkistrodon piscivorus piscivorus* (20 μL, 42 μM) or *Naja mossambica mossambica* (12 μL, 71 μM)) venom $sPLA_2$. Sampling was done after 0, 2, 24, and 48 h by collecting 100 μL of the reaction mixture and rapidly mixing it with a solution of $CHCl_3$/MeOH/H_2O/AcOH 4:8:1:1 (0.5 mL) in order to stop the reaction. The mixture was washed with water (0.5 mL), and the organic phase (80 μL) was isolated by extraction and then concentrated in vacuo. The extract was mixed with 9 μL of 2,5-dihydroxybenzoic acid (DHB) matrix (0.5 M DHB, 2 mM CF_3COONa, 1 mg/mL DPPG in MeOH), and 0.5 μL of this mixture was used for the MS analysis.

Cytotoxicity. Colon cancer HT-29 cells were cultured in McCoy's 5A medium in the presence of 10% fetal calf serum and 1% Pen-Strep (InVitrogen). Breast cancer MT-3 and colon cancer Colo205 cells were cultured in RPMI 1640 supplemented with 10% fetal calf serum and 1% Pen-Strep in a humidified atmosphere containing 5% CO_2. Colo205 cells secrete $sPLA_2$-IIa, however as the cytotoxicity assay was made with low cell density and for a short incubation period, inadequate concentrations were reached in the medium, which is why conditioned medium was used. Conditioned medium was made as follows: Colo205 cells were grown to confluency for 72 h, at which point the cells were pelleted and the medium, which contained approximately 100 ng/mL $sPLA_2$ IIA, was collected and used for the assay. Cells were plated in 96-well plates at a density of 1×10^4 cells per well for HT-29 and MT-3 cells and 2×10^4 cells per well for Colo205 cells, 24 h prior to addition of the tested compound. The retinoids (ATRA, **2**, **9**, **10**, and stearic acid) were solubilized in DMSO and water (final DMSO concentration ≤0.5%). Liposomes were diluted in PBS, and initial lipid concentrations in the liposome solutions were determined by phosphorus analysis.[50] After 24 h of incubation, the substances were removed and the cells were washed and incubated in complete medium for another 48 h. Cytotoxic activity was assessed using a standard 3-(4,5-dimethylthiazolyl)-2,5-diphenyltetrazolium bromide (MTT) assay (Cell Proliferation Kit I, Roche, Germany).[51] Cell viability is expressed as percentage reduction of incorporated MTT.

1-*O*-Octadecyl-2-(6-(all-*trans*-retinoyloxy)-hexanoyl)-*sn*-glycero-3-phospho-(*S*)-glycerol (3). Alcohol **15** (13 mg, 0.014 mmol), ATRA (6 mg, 0.019 mmol), and PPh_3 (9 mg, 0.043 mmol) were dissolved in THF (1.0 mL). DIAD (11 μL, 0.043 mmol) was added, and the reaction mixture was stirred at 20 °C for 1 h and then concentrated in vacuo and purified by flash column chromatography (heptane/EtOAc 2:1 then heptane/EtOAc 1:2) to give 13 mg that was dissolved in CH_2Cl_2 (1.0 mL) and DBU (2 μL, 0.012 mmol) was added. The reaction mixture was stirred for 30 min at 20 °C and then purified directly by flash column chromatography (heptane/EtOAc 1:1 then CH_2Cl_2/MeOH 9:1) to afford 8 mg that was dissolved in MeCN (0.9 mL) and CH_2Cl_2 (0.3 mL) and cooled to 0 °C. Aqueous HF (40%, 30 μL) was added dropwise, and the reaction mixture was allowed to reach 20 °C. After 3.5 h, the reaction was quenched by dropwise addition of $MeOSiMe_3$ (0.3 mL) and the mixture was stirred for 30 min, after which $NaHCO_3$ (6 mg, 0.07 mmol) was added and the mixture was concentrated in vacuo and purified by flash column chromatography (CH_2Cl_2/MeOH 10:1 then CH_2Cl_2/MeOH 4:1) to afford 4 mg (31% over 3 step) of **3** as a yellow amorphous solid. R_f = 0.44 (CH_2Cl_2/MeOH 4:1). ^{1}H NMR (500 MHz, $CDCl_3$/CD_3OD 4:1): δ 7.02 (dd, J = 15.0, 11.4 Hz, 1H), 6.32−6.27 (m, 2H), 6.15 (d, J = 11.4 Hz, 1H), 6.14 (d, J = 16.2 Hz, 1H), 5.77 (s, 1H), 5.18−5.13 (m, 1H), 4.11 (t, J = 6.6 Hz, 2H), 4.03−3.94 (m, 2H), 3.94−3.90 (m, 2H), 3.82−3.77 (m, 1H), 3.62 (t, J = 5.2 Hz, 2H), 3.60−3.57 (m, 2H), 3.49−3.39 (m, 2H), 2.39−2.33 (m, 5H), 2.05−2.00 (m, 5H), 1.72 (s, 3H), 1.71−1.60 (m, 6H), 1.57−1.51 (m, 2H), 1.50−1.45 (m, 2H), 1.45−1.40 (m, 2H), 1.31−1.23 (m, 30H), 1.03 (s, 6H), 0.88 (t, J = 6.9 Hz, 3H). ^{13}C NMR (50 MHz, $CDCl_3$/CD_3OD 4:1): δ 174.0, 168.0, 153.7, 140.0, 138.0, 137.7, 135.3, 131.7, 130.3, 129.8, 129.2, 118.5, 72.2 (2C), 71.2, 69.4, 66.7, 64.5, 64.1, 62.7, 40.0, 34.5 (2C), 33.4, 32.3, 30.1, 29.7 (12C), 29.2 (2C), 28.7, 26.4, 25.9, 24.9, 23.0, 22.0, 19.6, 14.3, 14.1, 13.3. IR (neat) 3325, 2923, 2853, 1733, 1709, 1609, 1584, 1457, 1259, 1064, 798 cm^{-1}; m/z (M + H$^+$) 917.58.

1-Octadecanoyl-2-(6-(all-*trans*-retinoyloxy)-hexanoyl)-*sn*-glycero-3-phospho-(*S*)-glycerol (4). Alcohol **18** (47 mg, 0.052 mmol), ATRA (31 mg, 0.104 mmol), DMAP (13 mg, 0.104 mmol), and Et_3N (72 μL, 0.52 mmol) were dissolved in Et_2O (1.2 mL). DCC (27 mg, 0.13 mmol) was added, and the reaction mixture was stirred at 20 °C for 22 h and then concentrated in vacuo and purified by flash column chromatography (toluene then toluene/EtOAc 5:1) to give 32 mg that was dissolved in CH_2Cl_2 (2.2 mL) and DBU (4.2 μL, 0.028 mmol) was added. The reaction mixture was stirred for 30 min at 20 °C and then purified directly by flash column chromatography (heptane/EtOAc 1:1 then CH_2Cl_2/MeOH 9:1) to afford 21 mg that was dissolved in MeCN (1.5 mL) and CH_2Cl_2 (0.5 mL) and cooled to 0 °C. Aqueous HF (40%, 90 μL) was added dropwise, and the reaction mixture was allowed to reach 20 °C. After 3.5 h, the reaction was quenched by dropwise addition of $MeOSiMe_3$ (0.3 mL) and the mixture was stirred for 30 min, after which $NaHCO_3$ (6 mg, 0.07 mmol) was added and the mixture was concentrated in vacuo and purified by flash column chromatography (CH_2Cl_2/MeOH 10:1 then CH_2Cl_2/MeOH 4:1 then CH_2Cl_2/MeOH/H_2O 65:25:1) to afford 15 mg (31% over 3 step) of **4** as a yellow amorphous solid. R_f = 0.56 (CH_2Cl_2/MeOH 5:1). ^{1}H NMR (500 MHz, $CDCl_3$/CD_3OD 4:1): δ 7.02 (dd, J = 15.0, 11.4 Hz, 1H), 6.32−6.27 (m, 2H), 6.15 (d, J = 11.4 Hz, 1H), 6.15 (d, J = 16.2 Hz, 1H), 5.77 (s, 1H), 5.25−5.20 (m, 1H), 4.39 (dd, J = 12.0, 3.3 Hz, 1H), 4.16 (dd, J = 12.0, 6.6 Hz, 1H), 4.11 (t, J = 6.6 Hz, 2H), 3.99−3.91 (m, 4H), 3.83−3.78 (m, 1H), 3.63 (t, J = 5.1 Hz, 2H), 2.36 (t, J = 7.5 Hz, 2H), 2.34 (s, 3H), 2.31 (t, J = 7.6 Hz, 2H), 2.05−2.00 (m, 5H), 1.71 (s, 3H), 1.71−1.65 (m, 4H), 1.65−1.57 (m, 4H), 1.50−1.45 (m, 2H), 1.45−1.41 (m, 2H), 1.34−1.21 (m, 28H), 1.03 (s, 6H), 0.88 (t, J = 7.0 Hz, 3H). ^{13}C NMR (50 MHz, $CDCl_3$/CD_3OD 4:1): δ 174.2, 173.5, 168.0, 153.6, 140.1, 138.0, 137.6, 135.3, 131.6, 130.3, 129.7, 129.1, 118.5, 71.2, 70.7, 66.8, 64.0 (2C), 62.6 (2C), 39.9, 34.3 (3C), 33.4, 32.2, 29.9 (12C), 29.2 (2C), 28.7, 25.8, 25.1, 24.8, 23.0, 21.9, 19.5, 14.3, 14.1, 13.1. ^{31}P NMR (202 MHz, $CDCl_3$/CD_3OD 4:1): δ −0.08. IR (neat): 3390, 2924, 2853, 1734, 1709, 1661, 1458, 1260, 1237, 1153, 1050, 805 cm^{-1}; m/z (M + H$^+$) 931.57.

1-*O*-Octadecyl-2-(6-(4′-octyl-4-phenylbenzoyloxy)-hexanoyl)-*sn*-glycero-3-phospho-(*S*)-glycerol (5). Alcohol **15** (62 mg, 0.068 mmol), carboxylic acid **2** (43 mg, 0.14 mmol), and DMAP (25 mg, 0.20 mmol) were dissolved in CH_2Cl_2 (4.5 mL). DCC (42 mg, 0.20 mmol) was added, and the reaction mixture was stirred at 20 °C for 18 h. The mixture was concentrated in vacuo and purified by flash column chromatography (toluene then toluene/EtOAc 5:1) to give 65 mg that was dissolved in CH_2Cl_2 (5.0 mL) and DBU (9 μL, 0.06 mmol) was added. The reaction mixture was stirred for 35 min at 20 °C and then purified directly by flash column chromatography (heptane/EtOAc 1:1 then CH_2Cl_2/MeOH 10:1) to afford 58 mg that was dissolved in a mixture of MeCN (4.2 mL) and CH_2Cl_2 (1.4 mL) and cooled to 0 °C. Aqueous HF (40%, 250 μL) was added dropwise, and the reaction mixture was allowed to reach 20 °C. After 3.5 h, the reaction was quenched by dropwise addition of $MeOSiMe_3$ (0.93 mL), and the mixture was stirred for 30 min, after which $NaHCO_3$ (8 mg, 0.095 mmol) was added and the mixture was concentrated in vacuo and purified by flash column chromatography (CH_2Cl_2/MeOH 10:1 then CH_2Cl_2/MeOH 4:1) to afford 24 mg (38% over 3 step) of **5** as a colorless amorphous solid. R_f = 0.23 (CH_2Cl_2/MeOH 4:1). ^{1}H NMR (300 MHz, $CDCl_3$/CD_3OD 4:1): δ 8.08 (d, J = 8.3 Hz, 2H), 7.67 (d, J = 8.3 Hz, 2H), 7.55 (d, J = 8.1 Hz, 2H), 7.29 (d, J = 8.1 Hz, 2H), 5.19−5.14 (m, 1H), 4.34 (t, J = 6.6 Hz, 2H), 4.06−3.93 (m, 4H), 3.85−3.80 (m, 1H), 3.66−3.61 (m, 2H), 3.60−3.56 (m, 2H), 3.48−3.38 (m, 2H), 2.66 (t, J = 7.7 Hz, 2H), 2.40 (t, J = 7.5 Hz, 2H), 1.86−1.79 (m, 2H), 1.76−1.70 (m, 2H), 1.69−1.62 (m, 2H), 1.56−1.49 (m, 4H), 1.39−1.19 (m, 40H), 0.89 (t, J = 6.8 Hz, 3H), 0.88 (t, J = 6.9 Hz, 3H). ^{13}C NMR (50 MHz, $CDCl_3$/CD_3OD 4:1): δ 173.9, 167.3, 146.1, 143.6, 137.5, 130.3 (2C), 129.3 (2C), 128.9, 127.4 (2C), 127.1 (2C), 72.1 (2C), 71.3, 69.3, 66.7, 65.2, 64.6, 62.6, 35.9, 34.5, 32.1 (2C), 31.8, 30.0, 29.7 (15C), 28.8, 26.3, 25.8, 24.9, 23.0 (2C), 14.3 (2C). ^{31}P NMR (202 MHz, $CDCl_3$/CD_3OD 4:1): δ −1.02. IR (neat): 3320, 2920, 2851, 1717, 1276, 1102, 1069 cm^{-1}; m/z (M + H$^+$) 927.58.

1-Octadecanoyl-2-(6-(4′-octyl-4-phenylbenzoyloxy)-hexanoyl)-*sn*-glycero-3-phospho-(*S*)-glycerol (6). The synthesis was performed as for **5**, starting from alcohol **18** (70 mg, 0.077 mmol) and affording 51 mg (70% over 3 step) of **6** as a colorless amorphous solid. R_f = 0.54 (CH_2Cl_2/MeOH 5:1). ^{1}H NMR (500 MHz, $CDCl_3$/CD_3OD 4:1): δ 8.08 (d, J = 8.3 Hz, 2H), 7.67 (d, J = 8.3 Hz, 2H), 7.56 (d, J = 8.1 Hz, 2H), 7.29 (d, J = 8.1 Hz, 2H), 5.27−5.22 (m, 1H), 4.39 (dd, J = 12.0, 3.2 Hz, 1H), 4.34 (d, J = 6.6 Hz, 2H), 4.17 (dd, J = 12.0, 6.6 Hz, 1H), 4.05−4.00 (m, 2H), 3.98−3.91 (m, 2H), 3.85−3.80 (m, 1H), 3.65−3.61 (m, 2H), 2.66 (t, J = 7.7 Hz, 2H), 2.40 (t, J = 7.5 Hz, 2H), 2.31 (t, J = 7.6 Hz, 2H), 1.86−1.78 (m, 2H), 1.76−1.69 (m, 2H), 1.68−1.62 (m, 2H), 1.62−1.56 (m, 2H), 1.55−1.49 (m, 2H), 1.39−1.20 (m, 38H), 0.89 (t, J = 6.7 Hz, 3H), 0.88 (t, J = 6.8 Hz, 3H). ^{13}C NMR (50 MHz, $CDCl_3$/CD_3OD 4:1): δ 174.4, 173.6, 167.4, 146.3, 143.7, 137.6, 130.4 (2C), 129.4 (2C), 129.0, 127.5 (2C), 127.2 (2C), 71.2, 70.8, 67.1, 65.2, 64.4, 62.7 (2C), 36.0, 34.4 (2C), 32.3 (2C), 31.8, 29.9 (15C), 28.8, 25.9, 25.2, 24.9, 23.0 (2C), 14.3 (2C). ^{31}P NMR (202 MHz, $CDCl_3$/CD_3OD 4:1): δ −1.30. IR (neat): 3314, 2921, 2851, 1737, 1467, 1277, 1103 cm^{-1}; m/z (M + H$^+$) 941.55.

Acknowledgment. We would like to acknowledge Prof. Helena Danielson (Department of Biochemistry and Organic Chemistry, Uppsala University) for her assistance with the enzyme inhibition assays. The technical help of Lars Duelund (MEMPHYS, University of Southern Denmark) is much appreciated. We thank the Danish Council for Strategic Research (NABIIT Program) for financial support. MEMPHYS-Center for Biomembrane Physics is supported by the Danish National Research Foundation.

Supporting Information Available: Analytical and spectral data for all synthesized compounds, experimental procedures for the synthesis of **2**, **7**, **9**, **10**, **14**, **15**, **17**, **18**, and 1-*O*-DSPG, Mosher ester analysis data of **17**, DLS analysis, further MALDI-TOF MS data for $sPLA_2$ degradation experiments, experimental procedures for the inhibition experiments and figures from MD simulations. This material is available free of charge via the Internet at http://pubs.acs.org.

References

(1) Barua, A. B.; Furr, H. C. Properties of Retinoids. *Mol. Biotechnol.* **1998**, *10*, 167–182.
(2) Rolewski, S. L. Clinical Review: Topical Retinoids. *Dermatol. Nurs.* **2003**, *15*, 447–465.
(3) (a) Okuno, M.; Kojima, S.; Matsushima-Nishiwaki, R.; Tsurumi, H.; Muto, Y.; Friedman, S. L.; Moriwaki, H. Retinoids in Cancer Chemoprevention. *Curr. Cancer Drug Targets* **2004**, *4*, 285–298. (b) Freementle, S. J.; Spinella, M. J.; Dmitrovsky, E. Retinoids in cancer therapy and chemoprevention: promise meets resistance. *Oncogene* **2003**, *22*, 7305–7315.
(4) (a) Huang, M. E.; Ye, Y. C.; Chen, S. R.; Chai, J.; Lu, J. X.; Zhoa, L.; Gu, L. J.; Wang, Z. Y. Use of all-*trans* retinoic acid in the treatment of acute promyelocytic leukemia. *Blood* **1988**, *72*, 567–572. (b) Castaigne, S.; Chomienne, C.; Daniel, M. T.; Ballerini, P.; Berger, R.; Fenaux, P.; Degos, L. All-trans retinoic acid as a differentiation therapy for acute promyelocytic leukemia. I. Clinical results. *Blood* **1990**, *76*, 1704–1709. (c) Regazzi, M. B.; Iacona, I.; Gervasutti, C.; Lazzarino, M.; Toma, S. Clinical Pharmacokinetics of Tritinoin. *Clin. Pharmacokinet.* **1997**, *32*, 382–402.
(5) Muindi, J. R. F.; Frankel, S. R.; Huselton, C.; DeGrazia, F.; Garland, W. A.; Young, C. W.; Warrell, R. P. Clinical pharmacology of oral all-*trans*-retinoic acid in patients with acute promyelocytic leukemia. *Cancer Res.* **1992**, *52*, 2138–2142.
(6) (a) Shimizu, K.; Tamagawa, K.; Takahashi, N.; Takayama, K.; Maitani, Y. Stability and antitumor effects of all-*trans* retinoic acid-loaded liposomes contained sterylglucoside mixture. *Int. J. Pharm.* **2003**, *258*, 45–53. (b) Kawakami, S.; Opanasopit, P.; Yokoyama, M.; Chansri, N.; Yamamoto, T.; Okano, T.; Yamashita, F.; Hasdida, M.

Biodistribution Characteristics of All-trans Retinoic Acid Incorporated in Liposomes and Polymeric Micelles Following Intravenous Administration. *J. Pharm. Sci.* **2005**, *94*, 2606–2615. (c) Díaz, C.; Vargas, E.; Gätjens-Boniche, O. Cytotoxic effect induced by retinoic acid loaded into galatosyl-sphingosine containing liposomes on human hepatoma cell lines. *Int. J. Pharm.* **2006**, *325*, 208–115. (d) Suzuki, S.; Kawakami, S.; Chansri, N.; Yamashita, F.; Hasdida, M. Inhibition of pulmonary metastasis in mice by all-trans retinoic acid incorporated in cationic liposomes. *J. Controlled Release* **2006**, *116*, 58–63.

(7) (a) Pedersen, P. J.; Christensen, M. S.; Ruysschaert, T.; Linderoth, L.; Andresen, T. L.; Melander, F.; Mouritsen, O. G.; Madsen, R.; Clausen, M. H. Synthesis and Biophysical Characterization of Chlorambucil Anticancer Ether Lipid Prodrugs. *J. Med. Chem.* **2009**, *52*, 3408–3415. (b) Christensen, M. S.; Pedersen, P. J.; Andresen, T. L.; Madsen, R.; Clausen, M. H. Isomerization of all-(E)-Retinoic Acid Mediated by Carbodiimide Activation—Synthesis of ATRA Ether Lipid Conjugates. *Eur. J. Org. Chem.* **2009**, 719–724. (c) Linderoth, L.; Peters, G. H.; Madsen, R.; Andresen, T. L. Drug Delivery by an Enzyme-Mediated Cyclization of a Lipid Prodrug with Unique Bilayer-Formation Properties. *Angew. Chem., Int. Ed.* **2009**, *48*, 1823–1826.

(8) (a) Newton, D. L.; Henderson, W. R.; Sporn, M. B. Structure−Activity Relationships of Retinoids in Hamster Tracheal Organ Culture. *Cancer Res.* **1980**, *40*, 3413–3425. (b) Um, S. J.; Kwon, Y. J.; Han, H. S.; Park, S. H.; Park, M. S.; Rho, Y. S.; Sin, H. S. Synthesis and Biological Activity of Novel Retinamide and Retinoate Derivatives. *Chem. Pharm. Bull.* **2004**, *52*, 501–506. (c) Gediya, L. K.; Khandelwal, A.; Patel, J.; Belosay, A.; Sabnis, G.; Mehta, J.; Purushottamachar, P.; Njar, V. C. O. Design, Synthesis, and Evaluation of Novel Mutual Prodrugs (Hybrid Drugs) of All-trans-Retinoic Acid and Histone Deacetylase Inhibitors with Enhanced Anticancer Activities in Breast and Prostate Cancer Cells in Vitro. *J. Med. Chem.* **2008**, *51*, 3895–3904. (d) Ulukaya, E.; Wood, E. J. Fenretinide and its relation to cancer. *Cancer Treat. Rev.* **1999**, *25*, 229–235.

(9) Linderoth, L.; Andresen, T. L.; Jørgensen, K.; Madsen, R.; Peters, G. H. Molecular Basis of Phospholipase A_2 Activity toward Phospholipids with *sn*-1 Substitutions. *Biophys. J.* **2008**, *94*, 14–26.

(10) Camacho, L. H. Clinical applications of retinoids in cancer medicine. *J. Biol. Regul. Homeostatic Agents* **2003**, *17*, 98–114.

(11) (a) Maden, M. Retinoic Acid in the Development, Regeneration and Maintenance of the Nervous System. *Nat. Rev. Neurosci.* **2007**, *8*, 755–765. (b) Swift, C. B.; Hays, J. L.; Petty, J. W. Distinct Functions of Retinoic Acid Receptor Beta Isoforms: Implications for Targeted Therapy. *Endocr., Metab. Immune Disord.: Drug Targets* **2008**, *8*, 47–50.

(12) Zhuang, Y.; Faria, T. N.; Chambon, P.; Gudas, L. J. Identification and characterization of retinoic acid receptor beta2 target genes in F9 teratocarcinoma cells. *Mol. Cancer Res.* **2003**, *1*, 619–630.

(13) (a) Piu, F.; Gauthier, N. K.; Olsson, R.; Currier, E. A.; Lund, B. W.; Croston, G. E.; Hacksell, U.; Brann, M. R. Identification of novel subtype selective RAR agonists. *Biochem. Pharmacol.* **2005**, *71*, 156–162. (b) Lund, B. W.; Piu, F.; Gauthier, N. K.; Eeg, A.; Currier, E.; Sherbukhin, V.; Brann, M. R.; Hacksell, U.; Olsson, R. Discovery of a Potent, Orally Available and Isoform-Selective Retinoic Acid β2 Receptor Agonist. *J. Med. Chem.* **2005**, *48*, 7517–7519. (c) Lund, B. W.; Knapp, A. E.; Piu, F.; Gauthier, N. K.; Begtrup, M.; Hacksell, U.; Olsson, R. Design, Synthesis, and Structure−Activity Analysis of Isoform-Selective Retinoic Acid Receptor β Ligands. *J. Med. Chem.* **2009**, *52*, 1540–1545.

(14) Bonsen, P. P. M.; de Haas, G. H.; Pieterson, W. A.; van Deenen, L. L. Studies on Phospholipase A and its Zymogen from Porcine Pancreas. IV. The Influence of Chemical Modification of the Lecithin Structure on Substrate Properties. *Biochim. Biophys. Acta* **1972**, *270*, 364–382.

(15) (a) Buckland, A. G.; Wilton, D. C. Anionic phospholipids, interfacial binding and the regulation of cell functions. *Biochim. Biophys. Acta* **2000**, *1483*, 199–216. (b) Canaan, S.; Nielsen, R.; Ghomashchi, F.; Robinson, B. H.; Gelb, M. H. Unusual mode of binding of human group IIA secreted phospholipase A2 to anionic interfaces as studied by continuous wave and time domain electron paramagnetic resonance spectroscopy. *J. Biol. Chem.* **2002**, *277*, 30984–30990. (c) Houlihan, W. J.; Lohmeyer, M.; Workman, P.; Cheon, S. H. Phospholipid antitumor agents. *Med. Res. Rev.* **1995**, *15*, 157–223.

(16) (a) Houlihan, W. J.; Lohmeyer, M.; Workman, P.; Cheon, S. H. Phospholipid antitumor agents. *Med. Res. Rev.* **1995**, *15*, 157–223. (b) Andresen, T. L.; Jensen, S. S.; Madsen, R.; Jørgensen, K. Synthesis and Biological Activity of Anticancer Ether Lipids that are Specifically Released by Phospholipase A_2 in Tumor Tissue. *J. Med. Chem.* **2005**, *48*, 7305–7314.

(17) (a) Hsieh, C. C.; Yen, M. H.; Liu, H. W.; Lau, Y. T. Lysophosphatidylcholine induces apoptotic and non-apoptotic death in vascular smooth muscle cells: in comparison with oxidized LDL. *Atherosclerosis* **2000**, *151*, 481–491. (b) Masamune, A.; Sakai, Y.; Satoh, A.; Fujita, M.; Yoshida, M.; Shimosegawa, T. Lysophosphatidylcholine induces apoptosis in AR42J cells. *Pancreas* **2001**, *22*, 75–83. (c) Kogure, K.; Nakashima, S.; Tsuchie, A.; Tokumura, A.; Fukuzawa, K. Temporary membrane distortion of vascular smooth muscle cells is responsible for their apoptosis induced by platelet-activating factor-like oxidized phospholipids and their degradation product, lysophosphatidylcholine. *Chem. Phys. Lipids* **2003**, *126*, 29–38.

(18) Peters, G. H.; Møller, M. S.; Jørgensen, K.; Rönnholm, P.; Mikkelsen, M.; Andresen, T. L. Secretoty Phospholipase A2 Hydrolysis of Phospholipid Analogues is Dependent on Water Accessibility to the Active Site. *J. Am. Chem. Soc.* **2007**, *129*, 5451–5461.

(19) Scott, D. L.; White, S.; Otwinowski, Z.; Yuan, W.; Gelb, M. H.; Sigler, P. B. Interfacial Catalysis—The Mechanism of Phospholipase-A_2. *Science* **1990**, *250*, 1541–1546.

(20) *tert*-Butyl 6-hydroxyhexanoate (**11**) was synthesized according to the litterature. Larock, R. C.; Leach, D. R. Organopalladium Approaches to Prostaglandins. 3. Synthesis of Bicyclic and Tricyclic 7-Oxaprostaglandin Endoperoxide Analoguesnvia Oxypalladation of Norbornadiene. *J. Org. Chem.* **1984**, *49*, 2144–2148.

(21) Mitsunobu, O. The Use of Diethyl Azodicarboxylate and Triphenylphosphine in Synthesis and Transformation of Natural Products. *Synthesis* **1981**, 1–28.

(22) Kaul, R.; Brouillette, Y.; Sajjadi, Z.; Hansford, K. A.; Lubell, W. D. Selective *tert*-Butyl Ester Deprotection in the Presence of Acid Labile Protection Groups with $ZnBr_2$. *J. Org. Chem.* **2004**, *69*, 6131–6133.

(23) Borgulya, J.; Bernauer, K. Transformation of Carboxylic Acid *t*-Butyl Esters into the Corresponding Trimethylsilyl Esters or Free Acids under Nonacidic Conditions. *Synthesis* **1980**, 545–547.

(24) Compound **2** is commercially available (CAS no. 59662-49-6), but during this work, **2** was synthesized in one step from the corresponding nitrile (CAS no. 52709-84-9) by a NaOH mediated hydrolysis in 98% yield (see Supporting Information).

(25) Neises, B.; Steglich, W. Simple Method for the Esterification of Carboxylic Acids. *Angew. Chem., Int. Ed. Engl.* **1978**, *17*, 522–524.

(26) Gaffney, P. R. J.; Reese, C. B. Synthesis of naturally occurring phosphatidylinositol 3,4,5-triphosphate [PtdIns(3,4,5)P_3] and its diastereoisomers. *J. Chem. Soc., Perkin Trans. 1* **2001**, 192–105.

(27) Burgos, C. E.; Ayer, D. E.; Johnson, R. A. A New, Asymmetric Synthesis of Lipids and Phospolipids. *J. Org. Chem.* **1987**, *52*, 4973–4977.

(28) Batten, R. J.; Dixon, A. J.; Taylor, R. J. K. A New Method for Removing the *t*-Butyldimethylsilyl Protecting Group. *Synthesis* **1980**, 234–236.

(29) Qin, D.; Byun, H. S.; Bittman, R. Synthesis of Plasmalogen via 2,3-Bis-*O*-(4′-methoxybenzyl)-*sn*-glycerol. *J. Am. Chem. Soc.* **1999**, *121*, 662–668.

(30) Dale, J. A.; Mosher, H. S. Nuclear Magnetic Resonance Enantiomer Reagents. Configurational Correlations via Nuclear Magnetic Resonance Chemical Shifts of Diastereomeric Mandelate, *O*-Methylmandelate, and α-Methoxy-α-trifluoromethylphenylacetate (MTPA) Esters. *J. Am. Chem. Soc.* **1973**, *95*, 512–519.

(31) (a) Lichtenberg, D.; Barenholz, Y. Liposomes—Preparation, Characterization and Preservation. *Methods Biochem. Anal.* **1988**, *33*, 337–462. (b) Tirrell, D. A.; Takigawa, D. Y.; Seki, K. Interactions of synthetic polymers with cell-membranes and model membrane systems 7. pH sensitization of phospholipid-vesicles via complexation with synthetic poly(carboxylic acid)s. *Ann. N.Y. Acad. Sci.* **1985**, *446*, 237–248.

(32) McIntyre, J. C.; Sleight, R. G. Fluorescence assay for phospholipid membrane asymmetry. *Biochemistry* **1991**, *30*, 11819–11827.

(33) (a) Huster, D.; Muller, P.; Arnold, K.; Herrmann, A. Dynamics of membrane penetration of the fluorescent 7-nitrobenz-2-oxa-1,3-diazol-4-yl (NBD) group attached to an acyl chain of phosphatidylcholine. *Biophys. J.* **2001**, *80*, 822–831. (b) Langner, M.; Hui, S. W. Dithionite penetration through phospholipid bilayers as a measure of defects in lipid molecular packing. *Chem. Phys. Lipids* **1993**, *65*, 23–30.

(34) (a) Harvey, D. J. Matrix-Assisted Laser Desorption/Ionization Mass Spectrometry of Phospholipids. *J. Mass Spectrom.* **1995**, *30*, 1333–1346. (b) Schiller, J.; Arnhold, J.; Benard, S.; Müller, M.; Reichl, S.; Arnold, K. Lipid Analysis by Matrix-Assisted Laser Desorption and Ionization Mass Spectrometry: A Methodological Approach. *Anal. Biochem.* **1999**, *267*, 46–56. (c) Petković, M.; Muller, J.; Muller, M.; Schiller, J.; Arnold, K.; Arnhold, J. Application of matrix-assisted laser desorption/ionization time-of-flight mass spectrometry for monitoring the digestion of phosphatidylcholine by pancreatic phospholipase A_2. *Anal. Biochem.* **2002**, *308*, 61–70.

(35) Fawzy, A. A.; Wishwanath, B. S.; Franson, R. C. Inhibition of human nonpancreatic phospholipases A_2 by retinoids and flavonoids. Mechanism of action. *Agents Actions* **1988**, *25*, 394–400.

(36) Hope, W. C.; Patel, B. J.; Fiedler-Nagy, C.; Wittreich, B. H. Retinoids inhibit Phospholipase A_2 in human synovial fluid and arachidonic acid release from rat peritoneal macrophages. *Inflammation* **1990**, *14*, 543–559.
(37) Cunningham, T. J.; Maciejewski, J.; Yao, L. Inhibition of secreted phospholipase A2 by neuron survival and anti-inflammatory peptide CHEC-9. *J. Neuroinflammation* **2006**, *3*, 25.
(38) Nicke, B.; Kaiser, A.; Wiedernmann, B.; Riecken, E. O.; Rosewicz, S. Retinoic Acid Receptor α Mediates Growth Inhibition by Retinoids in Human Colon Carcinoma HT29 Cells. *Biochem. Biophys. Res. Commun.* **1999**, *261*, 572–577.
(39) (a) Geurts van Kassel, W. S. M.; Hax, W. M. A.; Demel, R. A.; de Gier, J. High Performance Liquid Chromatographic Separation and Direct Ultraviolet Detection of Phospholipids. *Biochim. Biophys. Acta* **1977**, *486*, 524–530. (b) Rivnay, B. Combined Analysis of Phospholipids by High-Performance Liquid Chromatography and Thin-Layer Chromatography. *J. Chromatogr.* **1984**, *294*, 303–315.
(40) Hansford, K. A.; Reid, R. C.; Clark, C. I.; Tyndall, J. D. A.; Whitehouse, M. W.; Guthrie, T.; McGeary, R. P.; Schafer, K.; Martin, J. L.; Fairlie, D. P. D-Tyrosine as a chiral precusor to potent inhibitors of human nonpancreatic secretory phospholipase A(2) (IIa) with antiinflammatory activity. *ChemBioChem* **2003**, *4*, 181–185.
(41) Bernstein, F. C.; Koetzle, T. F.; Williams, G. J.; Meyer, E. E.; Brice, M. D.; Rodgers, J. R.; Kennard, O.; Shimanouchi, T.; Tasumi, M. Protein Data Bank—Computer-Based Archival File for Macromolecular Structures. *J. Mol. Biol.* **1977**, *112*, 535–542.
(42) Phillips, J. C.; Braun, R.; Wang, W.; Gumbart, J.; Tajkhorshid, E.; Villa, E.; Chipot, C.; Skeel, R. D.; Kale, L.; Schulten, K. Scalable molecular dynamics with NAMD. *J. Comput. Chem.* **2005**, *26*, 1781–1802.
(43) Jorgensen, W. L.; Chandrasekhar, J.; Medura, J. D.; Impey, R. W.; Klein, M. L. Comparison of simple potential models for simulating liquid water. *J. Chem. Phys.* **1983**, *79*, 926–935.
(44) Grubmüller, H. *Solvate: a program to create atomic solvent models*. Electronic publication: http://www.mpibpc.gwdg.de/abteilungen/071/solvate/docu.html; accessed 02/11/2010.
(45) Feller, S. E.; Zhang, Y.; Pastor, R. W.; Brooks., B. R. Constant pressure molecular dynamics simulation: the Langevin piston method. *J. Chem. Phys.* **1995**, *103*, 4613–4621.
(46) (a) Darden, T.; York, D.; Pedersen, L. Particle mesh Ewald an Nlog(n) method for Ewald sums in large systems. *J. Chem. Phys.* **1993**, *98*, 10089–10092. (b) Darden, T.; York, D.; Pedersen, L. Particle mesh Ewald: an N-log(N) method for Ewald sums in large systems. *J. Chem. Phys.* **1995**, *103*, 8577–8593.
(47) Humphrey, W.; Dalke, A.; Schulten, K. VMD—Visual Molecular Dynamics. *J. Mol. Graphics* **1996**, *14*, 33–38.
(48) Mills, J. K.; Needham, D. Lysolipid incorporation in dipalmitoylphosphatidylcholine bilayer membranes enhances the ion permeability and drug release rates at the membrane phase transition. *Biochim. Biophys. Acta* **2005**, *1716*, 77–96.
(49) (a) de Carvalho, L. M.; Schwedt, G. Polarographic determination of dithionite and its decomposition products: kinetic aspects, stabilizers, and analytical application. *Anal. Chim. Acta* **2001**, *436*, 293–300. (b) Stutts, K. J. Liquid chromatographic assay of dithionite and thiosulfate. *Anal. Chem.* **1987**, *59*, 543–544.
(50) Chen, P. S.; Toribara, T. Y.; Warner, H. Microdetermination of phosphorus. *Anal. Chem.* **1956**, *28*, 1756–1758.
(51) Carmichael, J.; DeGraff, W. G.; Gazdar, A. F.; Minna, J. D.; Mitchell, J. B. Evaluation of a tetrazolium-based semiautomated colorimetric assay: assessment of chemosensitivity testing. *Cancer Res.* **1987**, *47*, 936–942.